Classification of hydronephrosis with dynamic MR urography

R. A. Jones[1,2], D. Grattan-Smith[1,2]

[1]Radiology, CHOA, Atlanta, GA, United States, [2]Radiology, Emory University, Atlanta, GA, United States

Introduction

Antenatal hydronephrosis is the most commonly detected anomaly on maternal ultrasound scans. Most cases resolve spontaneously but some children develop obstructive uropathy. The consequences of obstructive uropathy are variable but usually depend on the degree of obstruction. The goal of the management of hydronephrosis is the preservation of renal function. Safe and effective interventions exist for the correction of obstruction, but the necessity, and timing, of these interventions remains controversial. Currently, there is no imaging 'gold standard' that can accurately assess the degree of obstruction and hence identify kidneys at risk for a progressive loss of renal function. In this abstract the ability of MR urography to evaluate the degree of obstruction is assessed.

Materials and methods

A total of 126 children were studied using MR urography on a 1.5T Siemens symphony scanner. All of the children received intra-venous hydration with lactated Ringers solution prior to the study, the volume infused being equal to the NPO deficit. A bladder catheter was placed to ensure free drainage of the urinary system, children of less than seven years of age were sedated. Once the child had been placed on the scanner and scout and a navigated T2 weighted images had been obtained, intra-venous Lasix (1 ml/kg, max 20 ml) was administered. T1 and T2 weighted coronal images and a heavily T2 weighted respiratory gated FSE sequence were then acquired (the latter was used to generate a pre-contrast MIP of the urinary system). 15 minutes after the Lasix was administered 0.1 mmol/kg Gd-DTPA was injected after the acquisition of the three initial images of a 3D, T1 weighted dynamic acquisition. For the subsequent four and half minutes images were acquired every 15 seconds. Images were then acquired every minute for a further 10 minutes, MIPs of each dynamic volume were automatically generated. 3D coronal, sagittal and axial images with high spatial resolution were then acquired for the purpose of generating a post-contrast MIP. In cases where the drainage of the contrast into the ureters was clearly delayed the patient was turned prone and a further set of coronal images was acquired. The renal transit time was calculated as the time between the cortical phase and the appearance of the contrast in the ureter. For a subset of 64 children the images best representing the cortical phase of the signal enhancement and the point when the medulla and cortex become isointense were selected and used as a basis for segmenting the cortex and parenchyma, subtraction was then used to derive the medullary volume. The cortical, medullary and parenchymal volumes and their corresponding split renal functions were calculated. In those children where a review of the dynamic images showed little or no motion (typically children under three years of age) the signal in the images was converted to relative signal by dividing the signal by the mean pre-contrast signal. Time-intensity curves for the cortex and medulla were then generated. The peak cortical and medullary relative signal (PRS) for each kidney were derived from the time-intensity curves and the initial slope of the post-peak wash-out (WOS) of the signal was measured by assuming this could be modeled as a linear function. The time at which the medullary signal exceeds the cortical signal was also estimated.

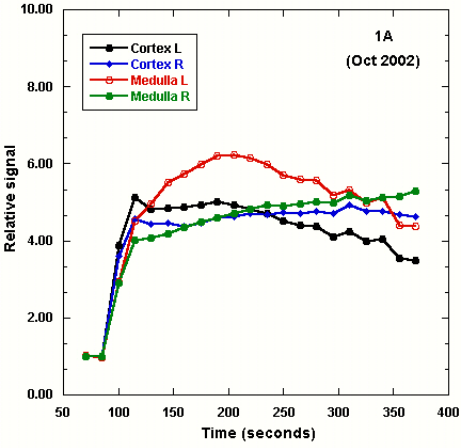

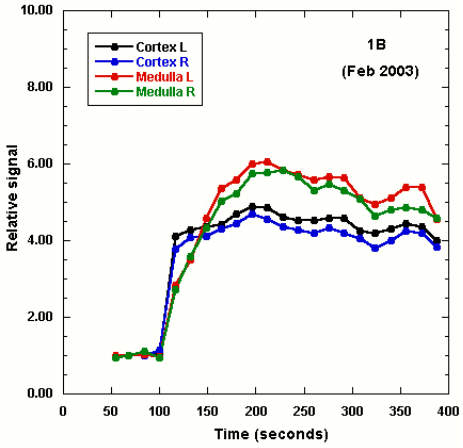

Results

The renal transit time was evaluated in 126 children, a histogram analysis was used to derive the limits for the normal values of the RTT (< 245 seconds), longer renal transit times were classified as either equivocal (245<RTT<=490 s) or obstructed (RTT>490s). Intra and inter-observes studies using linear regression both had r^2>0.99, indicating the technique is both robust and reliable. A ROC analysis comparing MRI and diuretic renal scintigraphy in 30 children showed good agreement between the modalities, with a mean area under the curve of 0.915. The crossover point was similar for patients with normal and equivocal RTTs but increased by approx. 15% for patients with a RTT in the obstructed category. The values derived from the time-intensity curves were categorised according to the RTT of the kidneys and are summarised in table 1, along with ratio of these quantities in cases where there was a normal kidney for comparison purposes. Figures 1A and 1B show the relative signal curves for a patient who underwent a pyeloplasty of the right kidney in the interval between the two studies, the curves show a clear recovery of renal function following pyeloplasty.

Table 1

	Cx. Normal	Cx. Equivocal	Cx. Obstructed	Med. Normal	Med. Equivocal	Med. Obstructed
WOS	0.49±0.12	0.38±0.14	0.31±0.14	0.69±0.22	0.53±0.25	0.37±0.19
WOS ratio	1.12±0.20	0.85±0.26	0.59±0.20	1.12±0.36	0.74±0.39	0.43±0.25
PRS	5.49±0.80	5.37±0.71	5.11±0.74	7.40±1.09	7.04±1.53	6.53±0.25
PRS ratio	1.02±0.07	0.97±0.06	0.88±0.10	1.02±0.10	0.93±0.10	0.83±0.09

Conclusion MR urography provides valuable information on renal functions as well as excellent anatomic imaging. The techniques described here, when combined with recent developments in BOLD and diffusion imaging of the kidneys, have the potential to make MR urography the exam of choice for assessing obstruction in pediatric patients.